

# Dynamics of Subnanometer Pt Clusters Can Break the Scaling Relationships in Catalysis

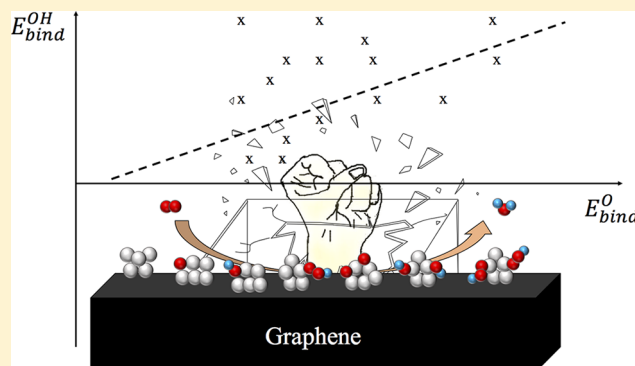
Borna Zandkarimi<sup>†</sup> and Anastassia N. Alexandrova<sup>\*,†,‡</sup>

<sup>†</sup>Department of Chemistry and Biochemistry, University of California, Los Angeles, Los Angeles, California 90095, United States

<sup>‡</sup>California NanoSystems Institute, Los Angeles, California 90095, United States

## Supporting Information

**ABSTRACT:** Scaling relationships in catalysis impose fundamental limitations on the catalyst maximal performance; therefore, there is a continuous hunt for ways of circumventing them. We show that, at the subnano-scale, scaling relationships can be broken through catalyst dynamics. Oxygen reduction reaction (ORR), which can be catalyzed by Pt nanoparticles, is used as our study case. Subnanometer gas-phase and graphene-deposited Pt<sub>n</sub> cluster catalysts are shown to exhibit poor correlation between binding energies of the intermediates, O, OH, and OOH, involved in the scaling relationships for ORR. The effect is due to the highly fluxional behavior of subnanometer clusters, which easily adapt their structures to the bound adsorbates and varying coverage and in some cases even reshape the structure upon changing environment. This fluxional behavior is also commonplace for clusters and contrasts them to extended surfaces, suggesting that breaking scaling relationships is likely a rule more than an exception in nanocluster catalysis.



Scaling relationships in catalysis provide a simple linear relationship between thermodynamic properties of chemically related species involved in a catalyzed reaction, across a range of catalytic surfaces. Examples include correlations between NH and NH<sub>2</sub> binding energies in ammonia synthesis and between O, OH, and OOH in oxygen reduction reaction (ORR). These simple but elegant relations have drawn the attention of many researchers in catalysis.<sup>1–9</sup> Although this simplicity leads to the ability to describe catalytic systems in terms of simple descriptors, such as the position of the d-band center and coordination numbers, scaling relations put an intrinsic limitation on the catalyst maximum activity. In fact, volcano plots are the results of linear relations between the kinetics and thermodynamics of the catalyzed reaction, implying that there is a maximum (at the top of the volcano) for the catalytic activity for each reaction.<sup>1,2,5,10,11</sup> Hence, there have been some efforts to find ways to break the scaling relationships and thus enhance the catalytic performance beyond the imposed maximum.<sup>12–14</sup> Here, we explore the properties of subnano Pt clusters in the nonscalable regime, i.e., a regime where properties change nonmonotonously with changes in cluster size, in the context of ORR catalysis as an example. We show that small Pt clusters do not necessarily follow a highly correlated linear relation and can potentially break the scaling relations, opening opportunities for outstanding catalytic performance.

The mechanism of ORR has been extensively investigated in the past.<sup>15–25</sup> It is known that platinum nanoparticles can

catalyze ORR.<sup>26–28</sup> Although nanoparticles with smaller size, around 1 nm, cannot efficiently catalyze ORR because of poisoning,<sup>29</sup> it has been shown that Pt subnano clusters catalyze ORR at an even higher rate than nanoparticles.<sup>30–32</sup> Both gas-phase and surface-deposited Pt subnanometer clusters have been studied theoretically and experimentally for the catalysis of ORR.<sup>31,33,34</sup> Because the mechanism of this reaction is the same in the solution and in the gas phase<sup>35</sup> and the gas-phase case is more computationally feasible, gas-phase Pt clusters have been more attractive for theoretical studies. Moreover, the approach is justified by the fact that graphene, being a suitable electrode material, causes no significant change to the geometries of the gas-phase Pt clusters, such as Pt<sub>13</sub>, upon deposition.<sup>35</sup> This study considers gas-phase and graphene-deposited Pt<sub>n</sub> clusters of varying sizes and addresses the ORR scaling relations in the subnano regime.

For ORR, different mechanisms have been proposed in acidic and alkaline solutions, among which the four-electron process in acidic solution can be written as<sup>36</sup>



In the dissociative mechanism of the reaction, O, OH, and OOH are the involved intermediates.<sup>17</sup> These are also the species whose binding energies to the catalysts typically

**Received:** December 8, 2018

**Accepted:** January 11, 2019

**Published:** January 11, 2019

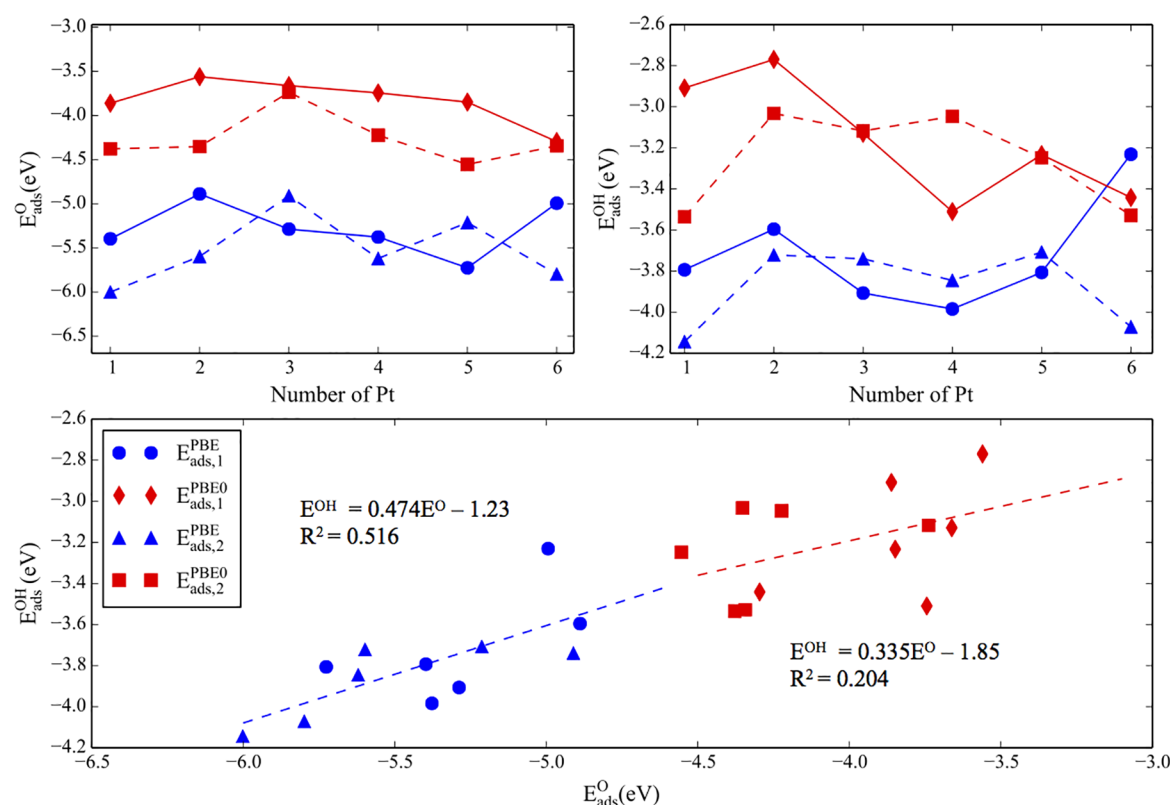


**Figure 1.** Scaling relationship between OH and O binding energies. The blue and red data sets correspond to the PBE and PBE0 calculations, respectively. Upper panel: the changes in the adsorption energies of O (left) and OH (right) as a function of cluster size. The binding energies of the first adsorbate are connected with the solid line, and the binding energies of the second adsorbate binding to the cluster are connected with a dashed line. Lower panel: correlations of the O and OH binding energies, computed with PBE and PBE0, in blue and red, respectively. Data points represent all studied cluster sizes and both coverages. The  $R^2$  values showcase the poor correlations. The slope of the line is far from the expected 0.5. Also, MAE for PBE data points is 0.12 eV and for PBE0 data points is 0.19 eV. MUE does not give a meaningful result because of the cancelation of error.

correlate. In this study we show that the correlation between the binding energies of each pair of these molecular fragments to Pt subnano clusters is weak, and the reason is the structural fluxionality of clusters that easily change upon changing adsorbate and coverage. Importantly, this is a test case, while the conclusions are potentially generalizable to other types of subnano clusters and other catalytic processes bound by scaling relations. Cluster dynamics emerges as a potential tool for circumventing scaling relations.

Figure 1 shows the correlation between the calculated OH and O binding energies to the gas-phase  $\text{Pt}_n$  ( $n = 1\text{--}6$ ) clusters. The binding energies are calculated for the first adsorbate binding to the cluster, and then also the second adsorbate of the same kind. Cluster geometries with and without bound adsorbates are found through global optimization of structures generated based on the bond length distribution algorithm (BLDA).<sup>37,38</sup> The geometries are in agreement with the ones obtained from the Birmingham parallel genetic algorithm (BPGA).<sup>39</sup> The adsorbate binding energies are calculated with respect to the gas-phase adsorbate and (i) the global minimum of the adsorbate-free cluster or (ii) the global minimum of the cluster with the first adsorbate bound, for the first and second adsorption energy calculations, respectively.

In the lower panel, the blue circles and triangles correspond to the binding energies of the first and second adsorbate, respectively, obtained from DFT calculations using the PBE functional. Because the effective valency changes from 2 for O

to 1 for OH, the expected slope of the line that relates their adsorption energies is 0.5. As can be seen, the slope of the line computed for the global minima of subnano clusters is deviated significantly from 0.5. The slope of the line indicates the contribution of the cluster to the optimal electron density of the bound atom, i.e., oxygen, in our case.<sup>1,2</sup> When the slope is significantly less than 0.5, this means that the cluster contributes less than expected to the oxygen electron density. The effect implies that the effective medium theorem might not be a good approximation for small clusters. In fact, this is not unexpected because the behavior of small clusters is far from metallic. Additionally, the  $R^2$  of 0.516 shows a poor correlation between data points. Moreover, mean absolute error (MAE) and mean unsigned error (MUE) have been calculated for both first and second binding energies. For PBE calculations, MAEs for all, first, and second binding energies are 0.12, 0.16, and 0.09 eV respectively. Note that mean unsigned errors (MUEs) for the first and second binding energies are  $-0.01$  and  $0.02$  eV, respectively, and will cancel out each other. The net result is that the predictability of the trend line might not be robust and reliable. The message holds true also for the PBE0 calculations, though in this case, the correlation is even worse ( $R^2 = 0.204$ ), and the deviation from the expected slope value of 0.5 is also larger (0.335). Furthermore, obtained MAEs for all, first, and second binding energies are 0.19, 0.20, and 0.18 eV, respectively. Again because of the different sign of MUE for the first and second binding energies ( $-0.03$  and  $0.03$  eV), they cancel out each

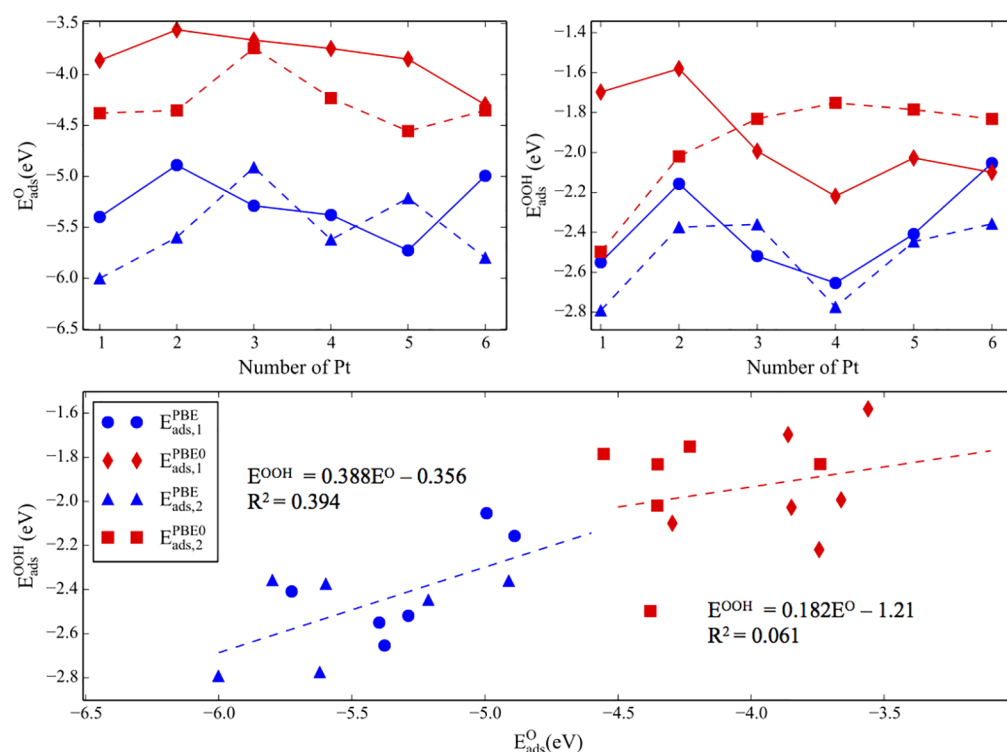


**Figure 2.** Scaling relationship between OOH and O binding energies. The blue and red data sets correspond to the PBE and PBE0 calculations, respectively. Color and style schemes and data types are analogous to those used in Figure 1. Also, MAE for PBE data points is 0.15 eV and for PBE0 data points is 0.20 eV. MUE does not give a meaningful result because of the cancelation of error.

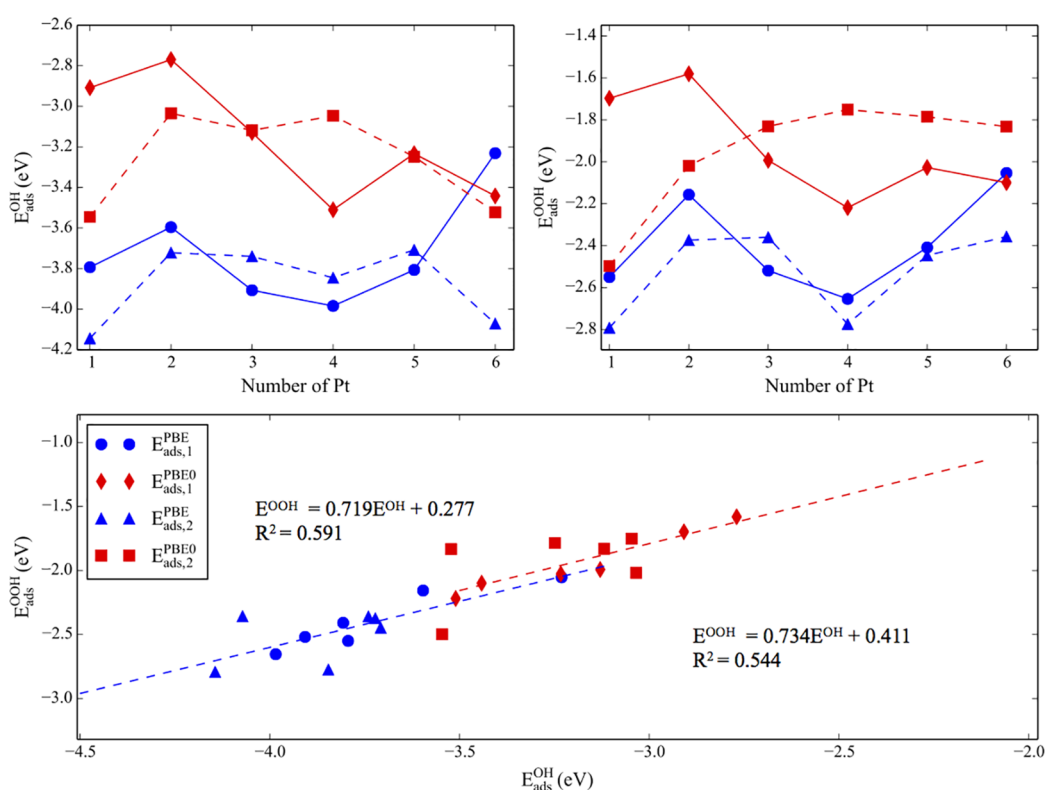


**Figure 3.** Scaling relationship between OOH and OH binding energies. Color and style schemes and data types are analogous to those used in Figure 1. The data points corresponding to the second binding adsorbate in the lower panel are more scattered, being responsible for the overall poor correlation, regardless of the functional. Also, MAE for PBE data points is 0.10 eV and for PBE0 data points is 0.12 eV. MUE does not give a meaningful result because of the cancelation of error.

other. The binding energies calculated with PBE0 are generally smaller, but the trends in cluster size correlate well with those calculated with PBE. Detailed discussion of the effect of functional on the results can be found in the [Supporting Information](#).

In order to illuminate the found poor correlations, we compare OH and O binding energy trends across the cluster sizes. In the upper panel, first and second binding energies are plotted as a function of number of Pt atoms. It is clear that OH and O binding energies do not have the same trends as a function of cluster size, resulting in the poor correlation. For instance, Pt<sub>5</sub> has the highest O binding energy, whereas Pt<sub>4</sub> has the highest OH binding energy ([Figure 1](#), upper panel, blue circles connected with the solid line). Furthermore, there is an increase in the O binding energy from Pt<sub>4</sub> to Pt<sub>5</sub>. On the other hand, the OH binding energy decreases from Pt<sub>4</sub> to Pt<sub>5</sub>. Similar observations can be made for the second adsorbate binding energies ([Figure 1](#), upper panel, blue triangles connected with the dashed line). Interestingly, however, the second adsorbate can bind to the cluster either more or less strongly than the first adsorbate, depending on the cluster size. For example, the second O binds to Pt<sub>4</sub> more strongly than the first O, and that is exactly opposite for the OH binding energy ([Figure 1](#), upper panel, blue lines).

The OOH and O binding energies and their correlations are shown in [Figure 2](#). Clearly the correlation is even worse than that for OH and O. The slope of the line obtained from PBE is 0.388 (compare with 0.474 for OH and O), and  $R^2$  is 0.394 (compare with 0.516 for OH and O). Again, the outcome of the PBE0 calculation is similar, but the predicted correlation is even worse. The slope of the line is again far from the expected 0.5 with both functionals, and the deviation is particularly drastic in PBE0.

[Figure 3](#) illustrates the scaling relationship between the OOH and OH binding energies. This particular correlation is the highest one obtained, with the  $R^2$  value of 0.591. However, this value is still very low compared to that for metallic surfaces, which is usually in the range of 0.8–0.95. Furthermore, in this case, the slope of the line is 0.719, which deviates significantly from the expected value of 1.0, given that the O atom binding to the cluster has the same valency in OH and OOH. Interestingly, the binding energies of the first adsorbed OOH and OH correlate quite well across cluster sizes ([Figure 3](#), upper panel, solid lines), leading to a stronger correlation. However, the effect of coverage is quite pronounced, and the binding energies for the second adsorbing OH and OOH exhibit very different trends ([Figure 3](#), upper panel, dashed lines). These higher coverage results are responsible for the overall poor correlation (seen in [Figure 3](#) bottom panel), and the failure of the scaling relationship. Coverage is not typically explored as a factor affecting scaling relations, but at least in the case of our clusters we see that it can be rather dramatic. The effect has to do with the cluster geometry change, and the change of the binding mode of OOH and OH when the second adsorbate binds, as discussed in detail below. Taken together, our findings so far suggest that small clusters can break the scaling relationship in catalysis and may exceed the intrinsic limit on catalytic activity.

[Figure 4](#) shows the global minimum structures of gas-phase Pt clusters before the adsorption and upon binding the first and then the second adsorbate. These results were obtained with PBE0, and the corresponding PBE results are presented in the [Supporting Information](#) ([Figures S1–S3](#)). In general, the

global minimum structure can be functional-dependent. The PBE functional gives a more flat structure for gas-phase Pt<sub>4</sub>, Pt<sub>5</sub>, and Pt<sub>6</sub>, whereas PBE0 predicts more globular geometries. However, these differences do not change the main conclusions of this study. Also, we have seen in the past that in thermal catalysis ensembles of many thermally accessible catalyst states collectively determine catalyst properties, such as electronic characteristics,<sup>40</sup> activity,<sup>41</sup> selectivity,<sup>42,43</sup> and sintering resistance.<sup>41–43</sup> Comparing the structures of Pt<sub>n</sub>O, Pt<sub>n</sub>OH, and Pt<sub>n</sub>OOH ( $n = 1–6$ ) sheds light on their binding energies not showing a strong correlation,<sup>40</sup> activity,<sup>41</sup> selectivity,<sup>42,43</sup> and sintering resistance.<sup>41–43</sup> In the present case, temperatures are milder, and the thermal ensembles of clusters states are small, with the vast majority of the population occupying the global minimum by Boltzmann statistics. For all cases reported in this work, the adsorption energies calculated as ensemble averages minimally differ from the results calculated based on just the global minima. We present the ensemble data in the [Supporting Information](#) ([Figures S4–S6](#)) and focus on the global minima in the main text.

The change in cluster shape is adsorbate-dependent, suggesting that the cluster should be changing shape in the course of the catalyzed ORR reaction. For instance, Pt<sub>5,6</sub> change geometries when one of O, OH, or OOH binds, and the geometry is every time different. We have seen such behavior for small catalytic Pt clusters in the past<sup>40–44</sup> and also found that cluster-shape change is exceptionally facile, allowing clusters visiting dozens of distinct minima in under 1 ns, even when on a supporting surface.<sup>45</sup> On the other hand, some clusters do not change shape so easily, such as Pt<sub>4</sub> and Pt<sub>4</sub>O, Pt<sub>4</sub>OH, and Pt<sub>4</sub>OOH. In fact, the cluster size-dependence of the fluxionality adds to the unpredictability (poor correlation) of binding energies. The highly dynamic behavior, which is also size- and composition-dependent, is unique to subnano clusters and certainly cannot be found in extended surfaces.

It is important to remark that in this work we operate under the assumption that the cluster has a chance to fully rearrange into an equilibrium thermodynamic ensemble in every minimum on the reaction profile. In other words, cluster dynamics is fast and decoupled from the reaction dynamics. This assumption is supported by our study of isomerization of Pt<sub>7</sub> on alumina, which appears to be exceptionally quick and structurally dramatic.<sup>45</sup> However, it is possible that this assumption is not generally applicable. Ideally, we would want to know how clusters isomerize and which cluster isomers are really linked to each other in the reaction profile of ORR. This computational task would be exceptionally demanding and is not within our reach.

Second, the poor correlations between the binding energies of O, OH, and OOH can be traced to the additional effect of the binding site change. In the scaling relationship, which was initially developed for extended surfaces, one usually assumes that the binding site does not change from surface to surface. However, as can be seen in [Figure 4](#), binding sites can change from one cluster size to another. For example, O preferentially binds on an atop site on Pt<sub>4</sub> but on a bridge site on Pt<sub>5</sub> and Pt<sub>6</sub>. Also, OOH preferentially binds using both of its oxygen atoms when on Pt<sub>2</sub>, Pt<sub>3</sub>, and Pt<sub>6</sub> but goes monodentate on the atop position when on Pt<sub>4</sub> and Pt<sub>5</sub>. In addition, O, OH, and OOH may preferentially bind to different sites on the same cluster. For example, O binds to the bridge site on Pt<sub>5</sub>, whereas OH and OOH prefer the atop site. For Pt<sub>6</sub>, O and OH bind on a



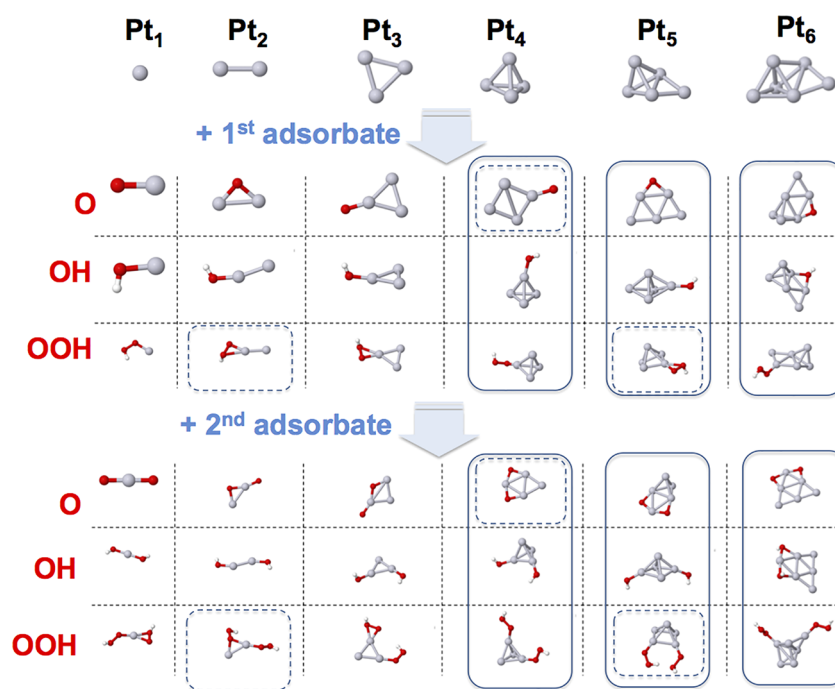


**Figure 4.** Global minimum structures of the gas-phase  $Pt_n$  ( $n = 1-6$ ) clusters without bound adsorbates and with one and then two bound adsorbates, O, OH, and OOH. Clusters outlined with solid lines change shapes when going from adsorbate-free to adsorbate-bound, often changing also from one adsorbate to another. Clusters outlined in dashed lines change the binding site of the adsorbate when the coverage changes. Gray, Pt; red, O; white, H.

bridge, and OOH binds atop. These changes are fundamentally not too surprising, because every atom in such small clusters is unique in its coordination geometry and electronic structure. For example, a bridge site on Pt<sub>4</sub> is electronically not the same as that on Pt<sub>5</sub>; every bridge site on every Pt<sub>n</sub> is unique, etc.

When the coverage increases, the situation changes again (Figure 4). The second adsorbate may bind to the bridge site or atop, depending on the cluster. The binding position is often different from that of the first adsorbate, meaning that their chemistries are going to be different. For instance, in Pt<sub>2</sub>O<sub>2</sub> and Pt<sub>3</sub>O<sub>2</sub>, and in Pt<sub>2</sub>(OOH)<sub>2</sub>, Pt<sub>3</sub>(OOH)<sub>2</sub>, and Pt<sub>5</sub>(OOH)<sub>2</sub>, the two adsorbates bind in two different sites, i.e., bridge and atop. Second, the second adsorbate can change the binding site of the first one. For instance, one O is bound atop on Pt<sub>4</sub>, but when two O atoms bind to Pt<sub>4</sub>, both of them go on the bridge site. Similarly, OH binds to Pt<sub>5</sub> on a bridge, but two OH bind atop in Pt<sub>5</sub>(OH)<sub>2</sub>. It is clear that the change in the cluster shape and electronic structure after the binding of the first adsorbate affects the binding site preference for the second adsorbate, and the second adsorbate in turn changes the cluster and affects the binding of the first adsorbate. In a steady state in catalysis, clusters would be covered by different adsorbates at concentrations dictated by the conditions and the adsorption strengths, and so our model reveals only part of the story. However, it is clear that every time an adsorbate comes, goes, or changes in the reaction, the catalyst itself changes too, altering all other adsorption energies and thus escaping the spell of the scaling relations.

To determine whether a similar behavior is characteristic of surface-deposited clusters, we choose to study at Pt<sub>5</sub> deposited on graphene, a support used as an electrode in ORR. Figure 5 shows the global minimum structures of Pt<sub>5</sub> on graphene, with and without the substrates, obtained via BH global optimization. Here too it can be seen that, when the adsorbate

binds to the cluster, it changes its shape, particularly in PBE calculations (see the Supporting Information) and particularly upon binding of the second adsorbate. The flat and upright shape of Pt<sub>5</sub> itself was seen also on MgO(100).<sup>46</sup> The second adsorbate can influence the preferred binding site for the first adsorbate. For instance, OH binds to the bridge site in Pt<sub>5</sub>OH, but as soon as the second OH binds, both adsorbates bind atop. Note the significant change in the structure of the cluster after the second OH binds to it. To determine whether a similar behavior is characteristic of surface-deposited clusters, we choose to study at Pt<sub>5</sub> deposited on graphene, a support used as an electrode in ORR. Figure 5 shows the global minimum structures of Pt<sub>5</sub> on graphene, with and without the adsorbates, obtained from basin hopping algorithm.<sup>47,48</sup> Here too it can be seen that, when the adsorbate binds to the cluster, it changes its shape, particularly with PBE (see the Supporting Information) and particularly upon binding of the second adsorbate. The flat and upright shape of Pt<sub>5</sub> itself was seen also on MgO(100).<sup>46</sup> The second adsorbate can influence the preferred binding site for the first adsorbate. For instance, OH binds to the bridge site in Pt<sub>5</sub>OH, but as soon as the second OH binds, both adsorbates bind atop. Note the significant change in the structure of the cluster after the second OH binds to it.

The computed binding energies for the surface-deposited cluster can be added to the trend lines shown in Figures 1–3. Doing this does not improve the trend and does not change the main conclusion (see Figure S7). The results suggest that small clusters, whether in the gas phase or on a supporting surface, would break scaling relations because of the changes in shape and in the adsorption binding sites, from one adsorbate to the next. We can also try to predict the adsorbate binding energies to the surface-deposited cluster from the trends obtained for the gas-phase clusters (Figures 1–3) and compare

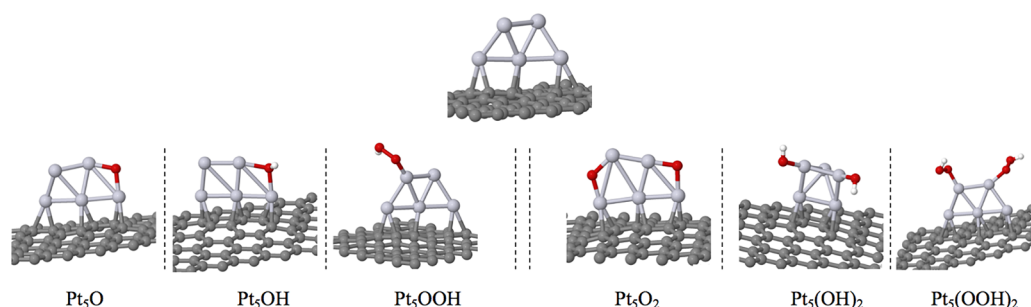


Figure 5. Global minimum structures for  $\text{Pt}_5$  cluster deposited on graphene with different adsorbates and coverage obtained with PBE0.

Table 1. Comparison of Calculated Binding Energies of Different Molecular Intermediates on  $\text{Pt}_5$  Deposited on Graphene with the Predicted Binding Energies Obtained from Gas-Phase Linear Scaling Relationships<sup>a</sup>

	$E_{\text{ads},1}^{\text{O}}(\text{eV})$	$E_{\text{ads},1}^{\text{OH}}(\text{eV})$	$E_{\text{ads},1}^{\text{OOH}}(\text{eV})$	$E_{\text{ads},2}^{\text{O}}(\text{eV})$	$E_{\text{ads},2}^{\text{OH}}(\text{eV})$	$E_{\text{ads},2}^{\text{OOH}}(\text{eV})$
calculated	−5.36	−3.63	−2.23	−5.23	−3.77	−2.42
predicted (from scaling)	− <sup>b</sup>	−3.77	−2.44	− <sup>b</sup>	−3.77	−2.44
error	—	0.14	0.21	—	0.00	0.02

<sup>a</sup>All results are obtained from PBE functional. <sup>b</sup>Reference state.

the outcome to the calculations. Table 1 shows the comparison. It is important to emphasize that the trend line does not distinguish between the first and second binding energies. Therefore, it can be argued that the average error for OH binding energy is 0.07 eV, and for OOH it is 0.12 eV, i.e. a factor of 2 smaller than what is reported in Table 1. Overall, even though a single example is not enough for statistics, we see the error in the binding energies varies depending on the adsorbate and can be significant or negligible in an unpredictable way.

It is obvious, however, that using just one example does not show whether the trend line obtained from gas phase can be applied to the surface deposited clusters. In fact, Figure S7 shows that the slope of the line deviates even more from the expected value (0.5 for OH vs O and 1.0 for OOH vs OH) when the surface-supported results are added.

In conclusion, because catalytic clusters at the subnano scale are exceptionally dynamic and easily change shapes upon binding different adsorbates, they break scaling relations that otherwise impose constraints on the maximal achievable catalytic performance. Depending on the cluster size, the change of shape upon binding and changing adsorbates and varying coverage may be greater or smaller. The binding sites of all adsorbates can be sensitive to the presence or absence of other adsorbates. As a result, correlations between the binding energies of adsorbates bound by scaling relations, such as O, OH, and OOH in ORR, become very loose, and their overall predictability becomes minimal. This is good news for catalysis, because it may allow optimizing catalysis beyond the current limits for such precious processes as ORR and ammonia synthesis. The levers at cluster catalyst design that may enable this optimization are (i) cluster size (because dynamics is cluster size-specific); (ii) reagent concentrations (because the binding sites and correlations are affected by coverage); and (iii) to some degree, also temperature (because cluster dynamics is enabled by thermal effects). Nanocatalysts are yet again unusual as compared to extended surfaces, in this newly found way.

## COMPUTATIONAL METHODS

Plane wave density functional theory calculations were performed using the Vienna Ab initio Simulation Package (VASP)<sup>49–52</sup> using projector augmented wave (PAW) potentials<sup>53</sup> and the PBE<sup>54</sup> functional. For the relaxation calculations presented in this Letter, large kinetic energy cutoffs of 400.0 eV and convergence criteria of  $10^{-6}$  eV were employed. Geometric relaxation was performed until forces on atoms were smaller than 0.01 eV/Å. Also, Gaussian smearing with the sigma value of 0.1 eV was used. Single-point calculations were done using the PBE0<sup>55,56</sup> functional on the structures obtained from the relaxation step using the PBE functional. The energy cutoff of 0.8 eV was used to filter local minima structures obtained from PBE calculation, which are then fed into PBE0 single-point calculation. Geometry relaxation of metal clusters using a hybrid functional, such as PBE0, usually causes some problem for the calculation to converge; however, geometries obtained from PBE calculations are usually reliable enough if a large enough energy cutoff is used to consider a significant number of local minima. A large unit cell of  $20 \text{ Å} \times 20 \text{ Å} \times 20 \text{ Å}$  was used for gas-phase calculations. Note that, for gas-phase calculations, in order to produce initial cluster geometries, we used our in-house code, PGOPT,<sup>37,40</sup> which automatically generates these structures based on the bond length distribution algorithm.<sup>37,38</sup> Then each structure was optimized using DFT calculation, and duplicates were filtered out thereafter. For  $\text{Pt}_5$  deposited on graphene, the basin hopping<sup>47,48</sup> algorithm implemented in PGOPT was used to determine the global and local minima structures. The experimental cell parameter of  $a = 2.46 \text{ Å}$  was used for graphene.<sup>57</sup> The unit cell was grown to a  $(6 \times 6)$  surface, and a vacuum gap of 15 Å was used. This results in a supercell with parameters of  $a = 14.76 \text{ Å}$ ,  $b = 14.76 \text{ Å}$ ,  $c = 20.0 \text{ Å}$ ,  $\alpha = 90^\circ$ ,  $\beta = 90^\circ$ , and  $\gamma = 120^\circ$ .  $\Gamma$ -point sampling was used for all calculations.

## ASSOCIATED CONTENT

### Supporting Information

The Supporting Information is available free of charge on the ACS Publications website at DOI: 10.1021/acs.jpcllett.8b03680.

Data obtained with PBE, scaling relations that include both gas-phase and surface-deposited clusters, and discussion on the performance of PBE versus PBE0 (PDF)

## AUTHOR INFORMATION

### Corresponding Author

\*E-mail: [ana@chem.ucla.edu](mailto:ana@chem.ucla.edu).

### ORCID

Borna Zandkarimi: 0000-0002-7633-132X

Anastassia N. Alexandrova: 0000-0002-3003-1911

### Notes

The authors declare no competing financial interest.

All coordinate files (XYZ and POSCAR format) of Pt<sub>5</sub>/graphene and gas-phase Pt clusters along with the description of each file (README.md) can be found at <https://github.com/bzkarimi/scaling-Pt-ORR>.

## ACKNOWLEDGMENTS

Our earlier work on cluster fluxionality, some of which appears in this paper, was supported by the Air Force Office of Scientific Research under a Basic Research Initiative grant (AFOSR FA9550-16-1-0141). The work relating to the ORR electrocatalysis was funded by DOE-BES grant DE-SC0019152. CPU resources at the DOD (Department of Defense) High Performance Computing Modernization Program [the U.S. Air Force Research Laboratory DoD Supercomputing Resource Center (AFRL DSRC), the U.S. Army Engineer Research and Development Center (ERDC), and the Navy Supercomputing Resource Center (Navy DSRC)], National Energy Research Scientific Computing Center (NERSC), a U.S. Department of Energy Office of Science User Facility operated under Contract No. DE-AC02-05CH11231, Extreme Science and Engineering Discovery Environment's (XSEDE) computing resources, and the UCLA-IDRE cluster were used to conduct this work.

## REFERENCES

- (1) Montemore, M. M.; Medlin, J. W. Scaling Relations between Adsorption Energies for Computational Screening and Design of Catalysts. *Catal. Sci. Technol.* **2014**, *4*, 3748–3761.
- (2) Greeley, J. Theoretical Heterogeneous Catalysis: Scaling Relationships and Computational Catalyst Design. *Annu. Rev. Chem. Biomol. Eng.* **2016**, *7*, 605–635.
- (3) Liu, J. X.; Su, Y.; Filot, I. A. W.; Hensen, E. J. M. A Linear Scaling Relation for CO Oxidation on CeO<sub>2</sub>-Supported Pd. *J. Am. Chem. Soc.* **2018**, *140*, 4580–4587.
- (4) Fernández, E. M.; Moses, P. G.; Toftelund, A.; Hansen, H. A.; Martínez, J. I.; Abild-Pedersen, F.; Kleis, J.; Hinnemann, B.; Rossmeisl, J.; Bligaard, T.; et al. Scaling Relationships for Adsorption Energies on Transition Metal Oxide, Sulfide, and Nitride Surfaces. *Angew. Chem., Int. Ed.* **2008**, *47*, 4683–4686.
- (5) Busch, M.; Wodrich, M. D.; Corminboeuf, C. Linear Scaling Relationships and Volcano Plots in Homogeneous Catalysis – Revisiting the Suzuki Reaction. *Chem. Sci.* **2015**, *6*, 6754–6761.
- (6) Jiang, T.; Mowbray, D. J.; Dobrin, S.; Falsig, H.; Bligaard, T. Trends in CO Oxidation Rates for Metal Nanoparticles and Close-Packed, Stepped, and Kinked Surfaces. *J. Phys. Chem. C* **2009**, *113*, 10548–10553.
- (7) Fu, Q.; Cao, X.; Luo, Y. Identification of the Scaling Relations for Binary Noble-Metal Nanoparticles. *J. Phys. Chem. C* **2013**, *117*, 2849–2854.
- (8) Calle-Vallejo, F.; Loffreda, D.; Koper, M. T. M.; Sautet, P. Introducing Structural Sensitivity into Adsorption-Energy Scaling

Relations by Means of Coordination Numbers. *Nat. Chem.* **2015**, *7*, 403–410.

(9) Calle-Vallejo, F.; Tymoczko, J.; Colic, V.; Vu, Q. H.; Pohl, M. D.; Morgenstern, K.; Loffreda, D.; Sautet, P.; Schuhmann, W.; Bandarenka, A. S. Finding Optimal Surface Sites on Heterogeneous Catalysts by Counting Nearest Neighbors. *Science* **2015**, *350*, 185–190.

(10) Quaino, P.; Juarez, F.; Santos, E.; Schmickler, W. Volcano Plots in Hydrogen Electrocatalysis-Uses and Abuses. *Beilstein J. Nanotechnol.* **2014**, *5*, 846–854.

(11) Sabatier, P. *La Catalyse En Chimie Organique*; Librairie Polytechnique: Paris, 1913.

(12) Gani, T. Z. H.; Kulik, H. J. Understanding and Breaking Scaling Relations in Single-Site Catalysis: Methane to Methanol Conversion by Fe<sup>IV</sup>=O. *ACS Catal.* **2018**, *8*, 975–986.

(13) Khorshidi, A.; Violet, J.; Hashemi, J.; Peterson, A. A. How Strain Can Break the Scaling Relations of Catalysis. *Nat. Catal.* **2018**, *1*, 263–268.

(14) Calle-Vallejo, F.; Krabbe, A.; García-Lastra, J. M. How Covalence Breaks Adsorption-Energy Scaling Relations and Solvation Restores Them. *Chem. Sci.* **2017**, *8*, 124–130.

(15) Nilekar, A. U.; Mavrikakis, M. Improved Oxygen Reduction Reactivity of Platinum Monolayers on Transition Metal Surfaces. *Surf. Sci.* **2008**, *602*, L89–L94.

(16) Shao, M.; Chang, Q.; Dodelet, J. P.; Chenitz, R. Recent Advances in Electrocatalysts for Oxygen Reduction Reaction. *Chem. Rev.* **2016**, *116*, 3594–3657.

(17) Tang, Z.; Wu, W.; Wang, K. Oxygen Reduction Reaction Catalyzed by Noble Metal Clusters. *Catalysts* **2018**, *8*, 65.

(18) Liu, M.; Zhang, R.; Chen, W. Graphene-Supported Nano-electrocatalysts for Fuel Cells: Synthesis, Properties, and Applications. *Chem. Rev.* **2014**, *114*, 5117–5160.

(19) Wong, W. Y.; Daud, W. R. W.; Mohamad, A. B.; Loh, K. S. Effect of Temperature on the Oxygen Reduction Reaction Kinetic at Nitrogen-Doped Carbon Nanotubes for Fuel Cell Cathode. *Int. J. Hydrogen Energy* **2015**, *40*, 11444–11450.

(20) Tse, E. C. M.; Gewirth, A. A. Effect of Temperature and Pressure on the Kinetics of the Oxygen Reduction Reaction. *J. Phys. Chem. A* **2015**, *119*, 1246–1255.

(21) Okaya, K.; Yano, H.; Kakinuma, K.; Watanabe, M.; Uchida, H. Temperature Dependence of Oxygen Reduction Reaction Activity at Stabilized Pt Skin-PtCo Alloy/Graphitized Carbon Black Catalysts Prepared by a Modified Nanocapsule Method. *ACS Appl. Mater. Interfaces* **2012**, *4*, 6982–6991.

(22) Li, D.; Lv, H.; Kang, Y.; Markovic, N. M.; Stamenkovic, V. R. Progress in the Development of Oxygen Reduction Reaction Catalysts for Low-Temperature Fuel Cells. *Annu. Rev. Chem. Biomol. Eng.* **2016**, *7*, 509–532.

(23) Keith, J. A.; Jacob, T. Theoretical Studies of Potential-Dependent and Competing Mechanisms of the Electrocatalytic Oxygen Reduction Reaction on Pt(111). *Angew. Chem., Int. Ed.* **2010**, *49*, 9521–9525.

(24) Chen, J.; Eguchi, K.; Waki, K. The Effect of Oxidation Temperature for the Oxygen Reduction Reaction Activity of Defective Multi-Walled Carbon Nanotubes (MWCNT). *ECS Trans.* **2017**, *80*, 677–684.

(25) Guo, S.; Zhang, S.; Sun, S. Tuning Nanoparticle Catalysis for the Oxygen Reduction Reaction. *Angew. Chem., Int. Ed.* **2013**, *52*, 8526–8544.

(26) Wu, J.; Yang, H. Platinum-Based Oxygen Reduction Electrocatalysts. *Acc. Chem. Res.* **2013**, *46*, 1848–1857.

(27) Huang, X.; Cao, L.; Chen, Y.; Zhu, E.; Lin, Z.; Li, M.; Yan, A.; Zettl, A.; Wang, Y. M.; Duan, X.; et al. High-Performance Transition Metal-Doped Pt<sub>3</sub>Ni Octahedra for Oxygen Reduction Reaction. *Science* **2015**, *348*, 1230–1234.

(28) Bu, L.; Zhang, N.; Guo, S.; Zhang, X.; Li, J.; Yao, J.; Wu, T.; Lu, G.; Ma, J. Y.; Su, D.; et al. Biaxially Strained PtPb/Pt Core/Shell Nanoplate Boosts Oxygen Reduction Catalysis. *Science* **2016**, *354*, 1410.



- (29) Shao, M.; Peles, A.; Shoemaker, K. Electrocatalysis on Platinum Nanoparticles: Particle Size Effect on Oxygen Reduction Reaction Activity. *Nano Lett.* **2011**, *11*, 3714–3719.
- (30) Imaoka, T.; Kitazawa, H.; Chun, W. J.; Yamamoto, K. Finding the Most Catalytically Active Platinum Clusters with Low Atomicity. *Angew. Chem., Int. Ed.* **2015**, *54*, 9810–9815.
- (31) Imaoka, T.; Kitazawa, H.; Chun, W. J.; Omura, S.; Albrecht, K.; Yamamoto, K. Magic Number Pt<sub>13</sub> and Misshapen Pt<sub>12</sub>clusters: Which One Is the Better Catalyst? *J. Am. Chem. Soc.* **2013**, *135*, 13089–13095.
- (32) Yamamoto, K.; Imaoka, T.; Chun, W. J.; Enoki, O.; Katoh, H.; Takenaga, M.; Sonoi, A. Size-Specific Catalytic Activity of Platinum Clusters Enhances Oxygen Reduction Reactions. *Nat. Chem.* **2009**, *1*, 397–402.
- (33) Miyazaki, K.; Mori, H. Origin of High Oxygen Reduction Reaction Activity of Pt<sub>12</sub> and Strategy to Obtain Better Catalyst Using Sub-Nanosized Pt-Alloy Clusters. *Sci. Rep.* **2017**, *7*, 45381–45390.
- (34) Nigam, S.; Majumder, C. ORR Viability of Alumina-Supported Platinum Nanocluster: Exploring Oxidation Behaviour by DFT. *Phys. Chem. Chem. Phys.* **2017**, *19*, 19308–19315.
- (35) Lim, D. H.; Wilcox, J. Mechanisms of the Oxygen Reduction Reaction on Defective Graphene-Supported Pt Nanoparticles from First-Principles. *J. Phys. Chem. C* **2012**, *116*, 3653–3660.
- (36) Wang, W.; Lei, B.; Guo, S. Engineering Multimetallic Nanocrystals for Highly Efficient Oxygen Reduction Catalysts. *Adv. Energy Mater.* **2016**, *6*, 1600236.
- (37) Pickard, C. J.; Needs, R. J. Ab Initio Random Structure Searching. *J. Phys.: Condens. Matter* **2011**, *23*, 053201–053223.
- (38) Pickard, C. J.; Needs, R. J. Structures at High Pressure from Random Searching. *Phys. Status Solidi B* **2009**, *246*, 536–540.
- (39) Demiroglu, I.; Yao, K.; Hussein, H. A.; Johnston, R. L. DFT Global Optimization of Gas-Phase Subnanometer Ru-Pt Clusters. *J. Phys. Chem. C* **2017**, *121*, 10773–10780.
- (40) Zhai, H.; Alexandrova, A. N. Ensemble-Average Representation of Pt Clusters in Conditions of Catalysis Accessed through GPU Accelerated Deep Neural Network Fitting Global Optimization. *J. Chem. Theory Comput.* **2016**, *12*, 6213–6226.
- (41) Baxter, E. T.; Ha, M. A.; Cass, A. C.; Alexandrova, A. N.; Anderson, S. L. Ethylene Dehydrogenation on Pt<sub>4,7,8</sub> Clusters on Al<sub>2</sub>O<sub>3</sub>: Strong Cluster Size Dependence Linked to Preferred Catalyst Morphologies. *ACS Catal.* **2017**, *7*, 3322–3335.
- (42) Ha, M. A.; Baxter, E. T.; Cass, A. C.; Anderson, S. L.; Alexandrova, A. N. Boron Switch for Selectivity of Catalytic Dehydrogenation on Size-Selected Pt Clusters on Al<sub>2</sub>O<sub>3</sub>. *J. Am. Chem. Soc.* **2017**, *139*, 11568–11575.
- (43) Jimenez-Izal, E.; Zhai, H.; Liu, J. Y.; Alexandrova, A. N. Nanoalloying MgO-Deposited Pt Clusters with Si to Control the Selectivity of Alkane Dehydrogenation. *ACS Catal.* **2018**, *8*, 8346–8356.
- (44) Zhai, H.; Alexandrova, A. N. Fluxionality of Catalytic Clusters: When It Matters and How to Address It. *ACS Catal.* **2017**, *7*, 1905–1911.
- (45) Zhai, H.; Alexandrova, A. N. Local Fluxionality of Surface-Deposited Cluster Catalysts: The Case of Pt<sub>7</sub> on Al<sub>2</sub>O<sub>3</sub>. *J. Phys. Chem. Lett.* **2018**, *9*, 1696–1702.
- (46) Shen, L.; Dadras, J.; Alexandrova, A. N. Pure and Zn-Doped Pt Clusters Go Flat and Upright on MgO(100). *Phys. Chem. Chem. Phys.* **2014**, *16*, 26436–26442.
- (47) Oganov, A. R. *Modern Methods of Crystal Structure Prediction*; Wiley-VCH Verlag GmbH & Co. KGaA: Weinheim, Germany, 2010.
- (48) Zhai, H. J.; Zhao, Y. F.; Li, W. L.; Chen, Q.; Bai, H.; Hu, H. S.; Piazza, Z. A.; Tian, W. J.; Lu, H. G.; Wu, Y. B.; et al. Observation of an All-Boron Fullerene. *Nat. Chem.* **2014**, *6*, 727–731.
- (49) Kresse, G.; Furthmüller, J. Efficiency of Ab-Initio Total Energy Calculations for Metals and Semiconductors Using a Plane-Wave Basis Set. *Comput. Mater. Sci.* **1996**, *6*, 15–50.
- (50) Kresse, G.; Hafner, J. Ab Initio Molecular Dynamics for Liquid Metals. *Phys. Rev. B: Condens. Matter Mater. Phys.* **1993**, *47*, 558–561.
- (51) Kresse, G.; Furthmüller, J. Ab Initio Molecular-Dynamics Simulation of the Liquid-Metal-Amorphous-Semiconductor Transition in Germanium. *Phys. Rev. B: Condens. Matter Mater. Phys.* **1994**, *49*, 14251–14269.
- (52) Kresse, G.; Furthmüller, J. Efficient Iterative Schemes for Ab Initio Total-Energy Calculations Using a Plane-Wave Basis Set. *Phys. Rev. B: Condens. Matter Mater. Phys.* **1996**, *54*, 11169–11186.
- (53) Kresse, G.; Joubert, D. From Ultrasoft Pseudopotentials to the Projector Augmented-Wave Method. *Phys. Rev. B: Condens. Matter Mater. Phys.* **1999**, *59*, 1758–1775.
- (54) Perdew, J. P.; Burke, K.; Ernzerhof, M. Generalized Gradient Approximation Made Simple. *Phys. Rev. Lett.* **1996**, *77*, 3865–3868.
- (55) Perdew, J. P.; Ernzerhof, M.; Burke, K. Rationale for Mixing Exact Exchange with Density Functional Approximations. *J. Chem. Phys.* **1996**, *105*, 9982–9985.
- (56) Adamo, C.; Barone, V. Toward Reliable Density Functional Methods without Adjustable Parameters: The PBE0Model. *J. Chem. Phys.* **1999**, *110*, 6158–6170.
- (57) Reddy, D.; Register, L. F.; Carpenter, G. D.; Banerjee, S. K. Graphene Field-Effect Transistors. *J. Phys. D: Appl. Phys.* **2011**, *44*, 313001–313020.